Journal of Nuclear Materials 392 (2009) 331–340

Contents lists available at ScienceDirect

Journal of Nuclear Materials

journal homepage: www.elsevier.com/locate/jnucmat

High temperature irradiation effects in selected Generation IV structural alloys

R.K. Nanstad [a,*], D.A. McClintock [b], D.T. Hoelzer [a], L. Tan [c], T.R. Allen [c]

[a] Materials Science and Technology Division, Oak Ridge National Laboratory, P.O. Box 2008, Oak Ridge, TN 37831-6138, USA
[b] University of Texas at Austin, 1 University Station C2200, Austin, TX 78712, USA
[c] University of Wisconsin, 1500 University Drive, Madison, WI 53706, USA

A B S T R A C T

In the Generation IV Materials Program cross-cutting task, irradiation and testing were carried out to address the issue of high temperature irradiation effects with selected current and potential candidate metallic alloys. The materials tested were (1) a high-nickel iron-base alloy (Alloy 800H); (2) a nickel-base alloy (Alloy 617); (3) two advanced nano-structured ferritic alloys (designated 14YWT and 14WT); and (4) a commercial ferritic–martensitic steel (annealed 9Cr–1MoV). Small tensile specimens were irradiated in rabbit capsules in the High-Flux Isotope Reactor at temperatures from about 550 to 700 °C and to irradiation doses in the range 1.2–1.6 dpa. The Alloy 800H and Alloy 617 exhibited significant hardening after irradiation at 580 °C; some hardening occurred at 660 °C as well, but the 800H showed extremely low tensile elongations when tested at 700 °C. Notably, the grain boundary engineered 800H exhibited even greater hardening at 580 °C and retained a high amount of ductility. Irradiation effects on the two nano-structured ferritic alloys and the annealed 9Cr–1MoV were relatively slight at this low dose.

1. Introduction

The behavior of advanced engineering materials under the conditions expected in Generation IV reactors is critical to the performance of those systems. In the case of materials utilized for reactor internals and pressure vessels, the effects of irradiation are major issues. The environmental conditions for most of the Generation IV reactors are generally beyond present day reactor technology, especially as regards the combinations of operating temperatures, reactor coolant characteristics, and neutron flux and spectra. In some of the applications, the conditions also are well beyond advanced research programs on radiation effects in materials. Therefore, new experimental data as well as analytical predictions of expected behavior of candidate materials at conditions for which there are no experimental data will be required. This paper includes significant new information, but is based on and includes most of the information in a paper electronically published in a conference proceedings [1].

The radiation environments and several key materials issues for the very high temperature reactor (VHTR), supercritical water reactor (SCWR), lead-cooled fast reactor (LFR) and gas-cooled fast reactor (GFR) are summarized in Section 5 of Ref. [2] as a starting point for modeling and microstructural analysis of Generation IV reactor materials. More detailed descriptions of materials research and development needs and recommended activities for the SCWR, VHTR, and GFR are provided in Refs. [3–5], respectively. From a different point of view, an interesting comparison of materials needs for Generation IV reactors to corresponding needs for fusion reactors and spallation neutron sources is available in Ref. [6]. Additionally, a detailed review of radiation effects in five classes of materials: (1) nickel-base alloys; (2) austenitic stainless steels; (3) ferritic–martensitic steels; (4) low alloy steels; and (5) refractory alloys, is provided in Ref. [7].

In general, structural alloys in these reactor concepts will be required to perform satisfactorily to doses ranging from 10s to 100 displacements per atom (dpa) or higher. The Next Generation Nuclear Plant (NGNP) concept, a VHTR, is different in this respect, however, because the graphite structure will moderate the fast neutron spectrum such that the irradiation doses to internal structures and the reactor pressure vessel (RPV) will be substantially lower than one dpa. Another common feature of the advanced reactor concepts is that they each require structural alloys within the reactor vessel to operate at high temperatures [8]. As discussed in Ref. [7], the temperatures range from 300 to 620 °C for the pressure vessel and core components of the SCWR and a proposed low temperature version of the LFR, and to 850 °C for the GFR core barrel. Under off-normal conditions, the temperatures of certain components could rise to as much as 1200–1600 °C in the GFR or VHTR.

In the Generation IV Materials Program cross-cutting task, plans were developed and irradiations and testing were carried out to address the issues associated with the effects of irradiation. This paper provides results for the first series of scoping irradiation experiments with selected metallic alloys, some of which are

* Corresponding author. Tel.: +1 865 574 4471; fax: +1 865 241 3650.
E-mail address: nanstadrk@ornl.gov (R.K. Nanstad).

0022-3115/$ - see front matter © 2009 Elsevier B.V. All rights reserved.
doi:10.1016/j.jnucmat.2009.03.022

considered candidate materials for Generation IV reactors, while others are considered as potential future candidate materials. The material classes represented are (1) a high-nickel iron-base alloy (Alloy 800H); a nickel-base alloy (Alloy 617); (3) two advanced nano-structured ferritic alloys (NFA) (designated 14WT and 14YWT); and (4) a commercial ferritic–martensitic steel (9Cr–1MoV). Relative to irradiation effects, the highly thermalized neutron environment and high temperature conditions for the VHTR internals present an operational regime that has received little attention. Additionally, the radiation response of the leading high strength, non-precipitation hardenable candidate alloys, such as Alloy 617 and Alloy 800H, are relatively unknown. A recent review of irradiation effects in nickel-base alloys can be found in Ref. [9]. There is a relatively large amount of radiation effects information on ferritic–martensitic steels, e.g., 9Cr–1MoV, but not at the higher temperatures. For the advanced NFA materials, there are no data on radiation effects at the high temperatures anticipated for the Generation IV reactors except for the results in Refs. [1,10].

2. Description of materials

The materials studied are Alloy 800H, Alloy 617, advanced NFA steels 14WT and 14YWT, and 9Cr–1MoV. The chemical compositions are provided in Tables 1–3. As shown in Table 1, although both Alloy 800H and Alloy 617 are very high in nickel content, major differences are that the 617 alloy has about 12% cobalt and Alloy 800H has about 45% iron. Because of the high nickel content, radioactivity will be quite high and will require testing in hot cells as well as special handling procedures for conduct of microstructural investigations. In the case of the Alloy 617, the cobalt content will present much greater problems in that regard and may render microstructural investigations impossible without very special facilities. The 800H was hot rolled and annealed by the producer (G.O. Carlson Inc.). Additionally, grain boundary engineering (GBE) was performed on Alloy 800H by means of thermomechanical processing by Tan et al. [11] at the University of Wisconsin–Madison (UW-Madison). Samples cut from the as-received material were subjected to a series of cold work (~6% thickness reduction) followed by a high temperature anneal (1050 °C for 90 min) and water quenching. The GBE treatment was employed primarily to improve the corrosion resistance, and to investigate the effect of GBE on radiation response. Tensile testing and microstructure characterization were performed by UW-Madison on the unirradiated GBE 800H, while tensile testing of the irradiated GBE 800H was performed by ORNL. Thermal aging indicated that the GBE optimized grain boundary character distribution is stable to 760 °C for 1000 h [11].

The Alloy 617 was provided in the solution annealed condition. This is a solid-solution-strengthened alloy, but precipitation of titanium nitrides and carbides provide additional strengthening. The 9Cr–1MoV was provided in the annealed condition and used in that condition to establish a baseline result for subsequent experiments with the material in various other heat treated conditions.

The advanced NFA materials were produced by ball-milling specially produced powder at ORNL [12,13]. These advanced NFAs, 14YWT and 14WT, exhibit unique microstructures. The 14YWT material is characterized by a high number density of ultrafine Ti-, Y-, and O-enriched particles, while the distribution of tungsten appears to be random in the interior of the grains [14]. Fig. 1 shows the grain structure and particle dispersions that were observed by TEM and energy-filtered TEM (EFTEM) analysis of 14WT (Fig. 1(a) and (b)) and 14YWT (Fig. 1(c) and (d)). The TEM analysis revealed a much smaller grain size of ~0.5 μm in 14YWT (Fig. 1(c)) as compared to ~1 μm in 14WT (Fig. 1(a)). However, the grains in both alloys were slightly elongated parallel to the extrusion direction with a length-to-width aspect ratio of ~1–5. An inhomogeneous distribution of carbides consistent with $M_{23}C_6$, where M is a mixture of Cr, Fe, and W was present in both alloys (i.e. two carbides are protruding from thinned regions in Fig. 1(a)). TEM bright field (BF) imaging and electron diffraction analysis combined with EFTEM were used for investigating the particle dispersions in the 14WT and 14YWT.

Elemental mapping of Fe obtained by EFTEM using the Fe M jump-ratio maps proved to be the most reliable method for detecting precipitates <2 nm diameter in Fe alloys. In 14WT, the BF images and selected area diffraction (SAD) analysis identified an inhomogeneous distribution of TiO_2 oxide particles that were typically larger than ~10 nm in diameter. In contrast, the techniques showed a very low number density of >10 nm size TiO_2 particles in 14YWT. However, the Fe M jump-ratio maps revealed a high number density of nano-size precipitates in 14YWT (Fig. 1(d)), but not in 14WT (Fig. 1(b)). The dark contrast associated with the nano-size precipitates is caused by locally lower Fe levels and depends on the thickness of the region. Also observed in the Fe M jump-ratio maps are the coarse TiO_2 particles, where 3 or 4 such particles are shown in 14YWT (Fig. 1(d)). As will be observed in Section 4, the nano-size particles result in extremely high tensile strengths for these materials.

3. Irradiation and testing procedures

The specimens were irradiated in rabbit capsules in the hydraulic tube of the ORNL High-Flux Isotope Reactor (HFIR). Each rabbit capsule was designed to hold eight SS-3 tensile specimens, a small plate specimen, silicon carbide (SiC) monitors for post-irradiation determination of the temperature during irradiation, and flux wires for determination of the irradiation dose. Dose measurements were subsequently used to calculate dpa. The plate specimen (0.5 mm thick) provided material for post-irradiation microstructural examinations, including transmission electron microscopy (TEM) and atom probe tomography (APT).

Electrical resistivity measurements of the SiC temperature monitors were used for the post-irradiation determinations of the irradiation temperatures for the specimens. As discussed in Ref. [15], electrical resistivity is considered to be an accurate and rapid method for such measurements over a temperature range

Table 2
Chemical compositions (wt%) of NFA ferritic alloy 14YWT and 14WT.

Material	Cr	Ni	Ti	W	B	Y_2O_3	O
14YWT	14	0.04	0.4	3.0	0.001	0.3	0.18
14WT	14	0.04	0.4	3.0	0.001		0.18

Table 1
Chemical compositions (wt%) of nickel-base alloys.

Material	Ni	Cr	Fe	Co	C	Mn	S	P	Si	Ti	Al	Mo
Alloy 800H[a]	31.6	20.4	45.3		0.07	0.76	0.001	0.014	0.35	0.57	0.50	
Alloy 617[b]	57.3	20.3	1.01	11.7	0.07	0.05	0.004		0.16		0.76	8.58

[a] G.O. Carlson Inc., Heat 35175, slab 2A.
[b] International Nickel Co., Heat XX01A3US.

Table 3
Chemical composition (wt%) of 9Cr–1Mo.

Material	C	Mn	S	P	Si	Cr	Ni	Al	Co	Mo	Cu	V	Nb
9Cr–1MoV[a]	0.081	0.37	0.003	0.01	0.11	8.61	0.09	0.007	0.010	0.89	0.04	0.21	0.07

[a] Heat 30176.

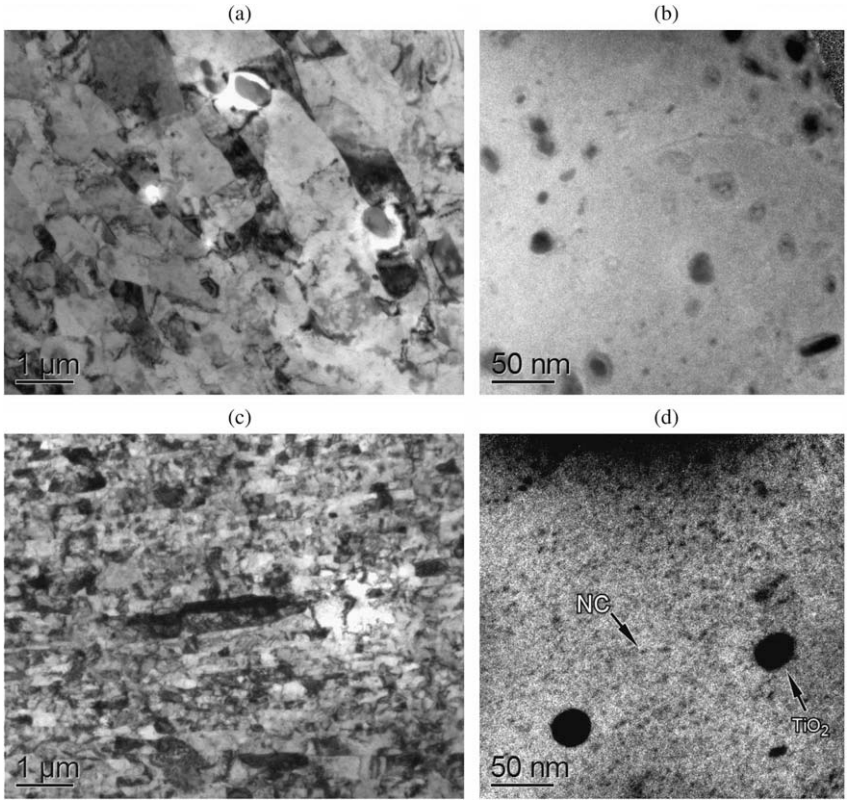

Fig. 1. The microstructures and particle dispersions of 14WT (a and b) and 14YWT (c and d). Bright-field TEM micrographs (a and c) and Fe M jump-ratio maps (b and d) with the arrow indicating a nanocluster (NC).

from ~200 to ~800 °C and for a dose range from ~0.1 to 8 dpa. The accuracy for this technique is given as <20 °C; thus, for the specimens irradiated in this project, the irradiation temperatures determined from the SiC monitors are considered accurate within 20 °C.

All mechanical property tests were conducted with flat SS-3 tensile specimens, 0.76 mm thick, 1.52 mm wide, and 25.4 mm long. The specimens are tested by loading on the shoulders of the specimen ends or by loading with pins placed through loading holes in the specimen ends. All specimens were tested in MTS servohydraulic machines with in-house developed computer programs, with the irradiated specimens tested in an ORNL hot cell. All tests were performed in machine displacement control at a rate of 0.51 mm/min. For each tensile test conducted, load and displacement measurements were used to determine the yield, ultimate, and fracture strengths, as well as the uniform and total elongations. Tests at elevated temperatures were conducted in air in a high temperature furnace capable of temperatures to 1200 °C. The specimen temperature during testing was monitored with a type S (Pt-Rh) thermocouple spot-welded to the specimen.

4. Results and discussion

4.1. Properties of unirradiated materials

Table 4 gives the tensile test results for all five materials, with the values shown being the average of the tests conducted at the indicated temperature. In most cases, the result is the average of two specimens. Tests were conducted to 900 °C for the two high-nickel alloys, to 650 °C for the annealed 9Cr–1MoV, and to 700 °C for the two NFA alloys. Fig. 2(a) and (b) compare the yield and ultimate strengths. The NFA 14YWT material has substantially higher strength than all the other materials, including the NFA 14WT. Yield strength and ultimate strength decrease with increasing test temperature, with the two NFA materials showing the most rapid decreases from room temperature strength. The NFA 14YWT exhibits an extremely high yield strength at room temperature, over 1400 MPa. Moreover, at 700 °C, the yield strength of the 14YWT material (435 MPa) is more than twice that of the other four materials and, as shown in Table 4, the total elongation is more than twice that of the 14WT material. This significant strengthening in the 14YWT material is attributed primarily to the much higher number density of nano-size precipitates compared with the 14WT material, as well as a lower number density of larger (>~10 nm diameter) TiO_2 oxide particles, as discussed in Section 2. For the two high-nickel alloys, Alloy 617 shows superior strength relative to the Alloy 800H at all temperatures to 900 °C. Fig. 3(a) and (b) show uniform and total elongation results for Alloy 800H and Alloy 617. Both alloys exhibit rapid decrease in uniform elongation with increasing temperatures above about 500 °C.

For the NFA materials, 14YWT and 14WT, tensile tests were performed at three different strain rates to investigate effects of strain rate on the tensile behavior. Tests were performed at 10^{-1}, 10^{-3},

Table 4
Tensile test results for all materials in the unirradiated condition.[a]

Material	Test temperature (°C)	Yield strength (MPa)	UTS (MPa)	Uniform elongation (%)	Total elongation (%)
9Cr–1MoV (annealed)	26	210.8	475.9	21.8	34.0
	400	172.0	353.3	13.8	25.4
	550	161.0	276.9	14.1	38.0
	650	112.6	163.9	11.7	68.9
Alloy 800H	26	263.2	535.4	45.0	53.7
	200	206.5	463.9	42.7	48.7
	400	173.9	463.4	49.6	59.5
	500	226.6	443.9	43.8	49.2
	600	234.4	424.1	35.2	43.5
	750	134.1	298.4	24.5	34.4
	800	119.8	223.8	18.2	42.5
	850	149.6	165.1	6.2	60.1
	900	116.0	124.9	3.1	56.2
Alloy 617	26	330.2	750.8	67.5	71.0
	200	272.7	664.3	68.2	71.0
	400	248.1	616.9	67.7	70.5
	500	234.8	607.8	68.6	75.0
	600	196.9	554.9	67.4	75.2
	750	196.2	487.9	50.2	67.7
	800	218.0	412.8	21.8	58.2
	900	207.1	450.4	36.0	62.9
14WT	26	743.0	934.7	11.0	21.3
	300	600.6	725.9	6.4	13.5
	500	509.3	568.4	4.3	16.9
	600	413.5	455.5	2.8	29.8
	700	177.6	226.9	2.5	50.0
14YWT	26	1435.2	1563.5	0.8	12.0
	300	1325.6	1384.2	0.7	8.0
	500	1033.7	1134.9	1.0	10.7
	600	693.6	782.9	1.9	19.2
	700	435.8	508.0	4.6	18.9

[a] In most cases, the values shown are averages of two tests.

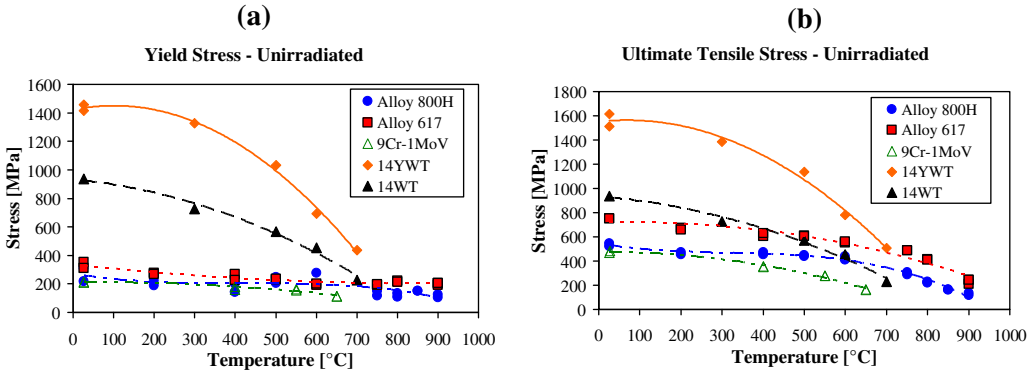

Fig. 2. Comparison of tensile test results for all five unirradiated materials showing: (a) yield strengths, and (b) ultimate strengths.

and 10^{-5}/s, and the yield strength results for 14YWT, not shown in this paper, demonstrate a tendency toward decreasing strength with decreasing strain rate, with the effect being greater at higher temperatures as the creep range is approached. The results for ultimate strength are similar.

4.2. Properties of irradiated materials

The neutron fluences (from hydraulic tube characterization values, not from rabbit capsule dosimeter) and calculated dpa results for the eight rabbit capsules irradiated in HFIR cycle 407 are given in Table 5. The nominal expected dose was 1.5 dpa, but neutron flux variations in the irradiation space resulted in dpa values from 1.28 to 1.61. The table also shows the material(s) in each capsule and the measured irradiation temperature for each capsule. The SiC monitors for the Alloy 617 capsules have not been evaluated, so the actual irradiation temperatures are assumed to be the same as those for the Alloy 800H.

The reported irradiation temperatures shown in Table 5 for the tensile specimens are based on evaluation of SiC monitors. Fig. 4 shows the SiC thermometry results for rabbit capsule N6C1, containing 14WT and 14YWT specimens irradiated at a target temperature of 600 °C. The figure shows the measurements given as the ratio of the electrical resistivity of the irradiated SiC monitor to that of a standard unirradiated SiC monitor measured at the same temperature. The specimens were annealed together and then measured with the same equipment. The dotted line in Fig. 4 represents the average of all the data denoted by filled circles, while

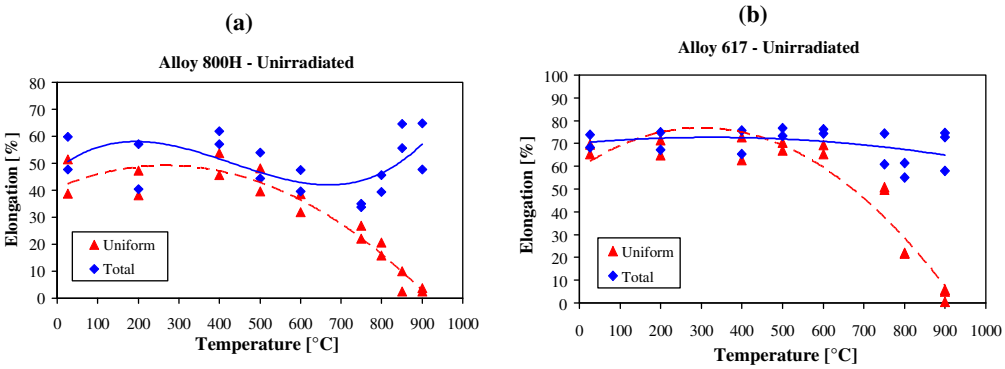

Fig. 3. Tensile test results showing elongations in the unirradiated condition for: (a) Alloy 800H and (b) Alloy 617.

Table 5
Irradiation fluence and displacements per atom (dpa) results for rabbit capsules.

					Fluence (n/cm^2)					
					E < 0.5 eV	0.5 eV–0.1 MeV	E > 0.1 MeV	E > 1 MeV		
Rabbit capsule	Material	Target irradiation temperature (°C)	Actual irradiation temperature (°C)	Location/axial position	Thermal	Epithermal	Fast	Fast-fast	Total	Dpa
N6C1	14YWT, 14WT	600	580	C1/2	2.86E + 21	2.17E + 21	1.79E + 21	8.41E + 20	7.65E + 21	1.28
N6D1	14YWT, 14WT	750	670	D5/3	4.79E + 21	1.17E + 21	1.71E + 21	8.38E + 20	8.51E + 21	1.22
N6E1	9Cr1MoV	550	570	A2/2	2.86E + 21	2.17E + 21	1.79E + 21	8.41E + 20	7.65E + 21	1.28
N6F1	9Cr1MoV	650	650	A3/2	2.86E + 21	2.17E + 21	1.79E + 21	8.41E + 20	7.65E + 21	1.28
N6G1	Alloy 800H	600	580	B5/2	2.86E + 21	2.17E + 21	1.79E + 21	8.41E + 20	7.65E + 21	1.28
N6H1	Alloy 800H	750	660	A4/5	3.44E + 21	2.74E + 21	2.26E + 21	1.11E + 21	9.55E + 21	1.61
N6I1	Alloy 617	600	580[a]	F7/2	2.86E + 21	2.17E + 21	1.79E + 21	8.41E + 20	7.65E + 21	1.28
N6J1	Alloy 617	750	660[a]	B1/4	3.49E + 21	2.64E + 21	2.18E + 21	1.03E + 21	9.34E + 21	1.56

[a] No SiC thermometry results available; the actual irradiated temperatures are assumed to be the same as those for the Alloy 800H.

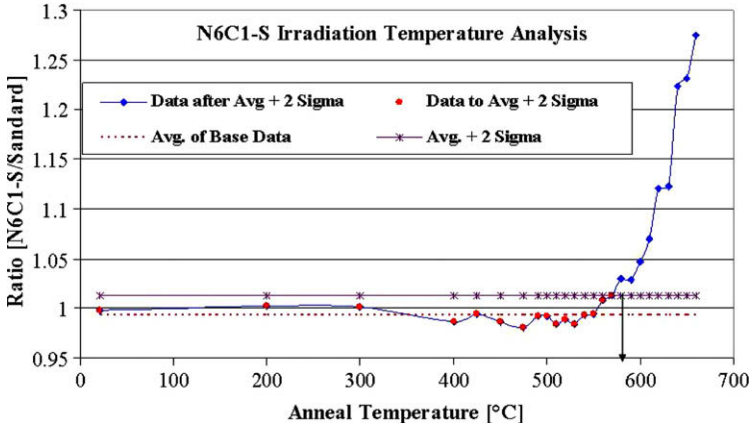

Fig. 4. SiC thermometer measurements and analysis for one rabbit capsule with a target irradiation temperature of 600 °C. Analysis show 580 °C was actual irradiation temperature.

the solid line represents the average plus one standard deviation (1). The best estimate of the irradiation temperature is the point at which the measurement exceeds the dotted line by 2. Thus, as shown in Table 5, the two capsules with a target irradiation temperature of 750 °C achieved temperatures 80–90 °C lower than the target. Therefore, the highest temperature tensile tests were conducted at this best estimate of the irradiation temperatures.

Table 6 summarizes the as-irradiated results for the five tested materials. (In some cases, two specimens were tested at a given temperature). Figs. 5–10 compare the yield and ultimate tensile strengths, as well as the uniform and total elongation values, for each material in the unirradiated and irradiated conditions.

For the Alloy 800H (Fig. 5), the hardening resulting from the 580 °C irradiation was significant, with increases in yield and ultimate strength on the order of 100% and 50%, respectively, in tests at room temperature. With increasing test temperature, the hardening decreased, but the yield strength increase was still about 50% for the 580 °C irradiation with tests at 550 °C. Results from the 660 °C irradiation of Alloy 800H show much less hardening, but

Table 6
Tensile test results for all materials in the irradiated condition.

Material	Specimen ID	Irradiation temperature (°C)	Test temperature (°C)	Yield strength (MPa)	Ultimate strength (MPa)	Total elongation (%)	Uniform elongation (%)
Alloy 617	7-2	580	25	597.9	923.5	38.8	37.5
	7-4		25	599.1	935.8	37.1	35.6
	7-10		400	512.5	829.3	37.0	36.0
	7-12		400	488.4	788.3	32.2	30.2
	7-15		500	493.7	769.5	32.9	30.3
	7-25		500	509.4	757.7	37.1	34.8
	7-27		580	481.1	776.4	28.8	27.7
	7-34		580	489.1	779.1	31.3	29.3
Alloy 617	7-3	660	25	524.4	933.1	35.8	34.1
	7-5		25	445.5	870.3	33.4	32.8
	7-7		400	404.9	793.3	31.9	30.5
	7-8		400	399.1	769.9	31.5	30.2
	7-9		600	381.1	686.8	28.5	26.6
	7-29		600	414.4	733.5	28.7	27.0
	7-33		700	364.3	570.7	15.3	13.5
	7-35		700	421.3	596.0	11.2	8.70
Alloy 800H	8-4	580	24	540.9	816.3	25.1	21.1
	8-5		24	567.7	810.5	21.9	18.0
	8-8		450	366.6	627.0	24.0	21.0
	8-9		450	318.7	594.9	24.2	22.5
	8-15		550	297.2	505.6	14.0	12.4
	8-28		580	356.2	524.4	10.6	7.90
	HG1		580	403.7	514.4	11.8	7.34
	AR2		580	272.0	362.4	12.9	8.05
Alloy 800H	8-1	660	24	258.9	556.2	35.9	29.0
	8-12		24	267.0	561.9	38.1	32.5
	8-13		450	271.2	525.9	21.3	18.3
	8-16		700	368.1	375.4	1.56	0.36
	8-30		660	237.9	368.5	8.88	6.33
	HG2		660	283.8	390.3	9.19	5.04
	AR1		660	249.4	371.9	9.55	6.11
9Cr–1MoV	91-3	570	24	219.9	472.3	33.6	19.5
	91-4		24	247.8	476.1	33.7	18.1
	91-5		300	207.6	415.6	32.0	18.3
	91-6		300	189.6	408.3	32.9	19.9
	91-7		400	208.4	396.1	29.5	17.5
	91-9		400	186.2	378.1	28.0	15.5
	91-11		500	148.2	329.8	25.9	14.2
	91-14		550	165.1	340.9	25.7	13.9
9Cr–1MoV	91-15	650	24	219.5	461.2	36.4	20.3
	91-16		24	226.8	466.5	35.0	19.9
	91-17		300	252.8	412.9	31.7	19.5
	91-18		300	205.3	407.2	34.1	19.8
	91-20		400	148.6	379.2	23.9	10.5
	91-21		400	165.5	375.0	28.7	17.6
	91-22		600	119.9	243.6	27.8	14.1
	91-23		650	197.3	204.2	20.9	0.98
14YWT	7-14, 1Y	580	24	1468.2	1652.8	7.28	1.05
	7-14, 2Y		500	1235.7	1328.8	7.46	0.88
	7-14, 3Y		550	1076.7	1179.0	7.59	0.87
	7-14, 4Y		580	936.5	1040.3	8.49	1.11
14YWT	7-9, 1Y	670	24	1442.5	1465.9	7.46	0.58
	7-9, 2Y		500	1224.6	1304.2	7.22	0.82
	7-9, 4Y		670	626.7	692.5	11.0	1.20
	7-9, 3Y		700	415.6	455.1	12.5	3.60
14WT	6-15, 1	580	24	650.8	881.4	18.9	10.0
	6-15, 2		500	543.9	702.5	14.4	6.87
	6-15, 3		550	460.8	532.4	16.0	5.18
	6-15, 4		580	473.8	535.1	12.7	3.42
14WT	6-8, 1	670	24	727.4	923.5	18.9	9.88
	6-8, 2		500	537.8	635.1	14.5	6.49
	6-8, 4		670	351.6	372.7	17.0	1.10
	6-8, 3		700	219.1	238.3	23.6	1.49

with extremely low tensile elongations, less than 0.5%, when tested at 700 °C. Fig. 6(a) and (b) show representative stress–strain curves for the Alloy 800H in the unirradiated condition and after irradiation at 660 °C. For the unirradiated material, the curves show a continual decrease of ultimate strength with increasing temperature, but also show that, although the total elongation similarly decreased to 750 °C, it then increased at 800 and 900 °C. The curves for specimens irradiated at 660 °C show a continual decrease in

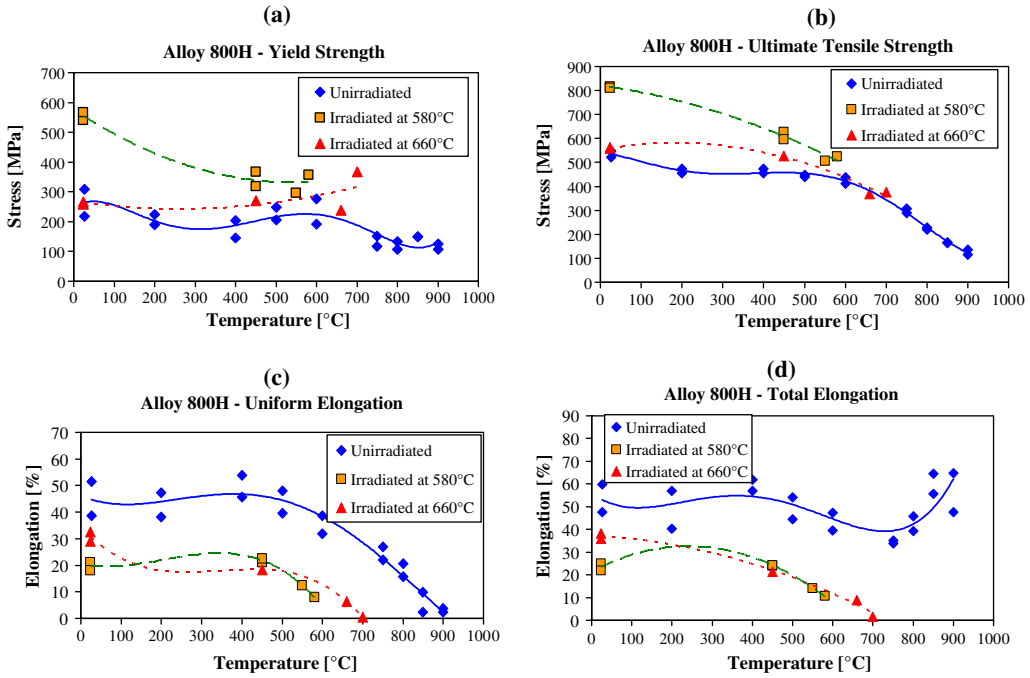

Fig. 5. Tensile test results for Alloy 800H: unirradiated and after irradiation to about 1.45 dpa, (a) yield stress, (b) ultimate tensile strength, (c) uniform elongation, and (d) total elongation.

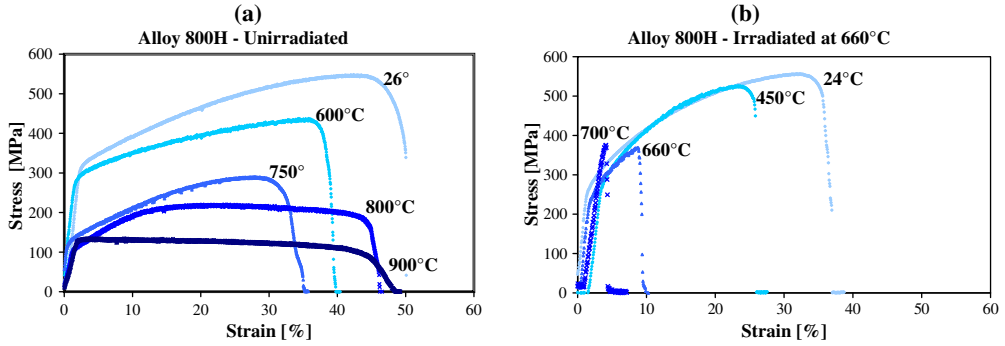

Fig. 6. Stress–strain curves for Alloy 800H: (a) unirradiated and (b) after irradiation at 660 °C to 1.45 dpa.

strength and in elongation with increasing test temperature and, as shown, the test at 700 °C has total elongation of only about 0.5% to failure.

Table 6 includes results for the GBE-treated specimens HG1 and HG2, and the as-received specimens AR1 and AR2. The GBE-treated specimens were irradiated at 580 or 660 °C and the results show significant irradiation-induced hardening at 580 °C, but much less at 660 °C. Notable, however, is that the strength increase of the GBE material irradiated at 580 °C is significantly greater than that of the as-received material, while the tensile ductilities are about the same (see Table 7).

For the Alloy 617 (Fig. 7), the yield strength increase was about 75–100% at all test temperatures for the 660 °C irradiation. For irradiation at 580 °C, the increases were even larger, ranging from 100% to 150% in tests at room temperature to 700 °C. Increases in ultimate strength of about 25% were also observed for this material, with the increases about the same for both irradiation temperatures. The changes in elongations for the Alloy 617 were substantial at both irradiation temperatures, with decreases of about 50%. However, unlike the Alloy 800H which experienced only 0.5% total elongation after irradiation, the total elongation for the Alloy 617 remained above 10% at 700 °C. For the tensile tests of the Alloy 617 in the irradiated condition, plastic instability was observed for the tests at about 500 and 600 °C, but not for the tests at 700 °C.

Results for the NFA 14YWT (Fig. 8) indicate about 20% increases in yield strength (ultimate strength is not shown but effects are similar) for tests in the range 500–600 °C, but no hardening is observed for tests at the lower temperatures or at 700 °C. Both the uniform and total elongations for 14YWT are decreased at both irradiation temperatures, but the total elongation (shown in Fig. 8) does not fall below 7% at any test temperature and increases to about 12% from 500 to 700 °C. For the NFA 14WT material (Fig. 9), there are insufficient results to make conclusions about irradiation-induced hardening below 500 °C, and the results for tests from 500 to 700 show no significant effect of irradiation on strength. The results for total elongation are similar to those for the 14YWT, except that the elongation is about twice as high for the 14WT material. Overall, the available data do not indicate significant effects of irradiation on hardening at this relatively low dose, but there are significant effects on tensile ductility, especially total elongation.

Table 7
Tensile test results for grain boundary engineered (GBE) Alloy 800H [10].

Irradiation test temperature (°C)	Specimen	Yield stress (MPa)	Ultimate stress (MPa)	Failure stress (MPa)	Total elongation (%)	Uniform elongation (%)
580	AR	272	362	61	13	8
	GBE	404[a]	514	53	12	7
	Change	48%	42%	−13%	−8%	−9%
660	AR	249	372	39	10	6
	GBE	284	390	48	9	5
	Change	14%	5%	25%	−4%	−17%

[a] This value is corrected from the typographical error reported in Ref. [10].

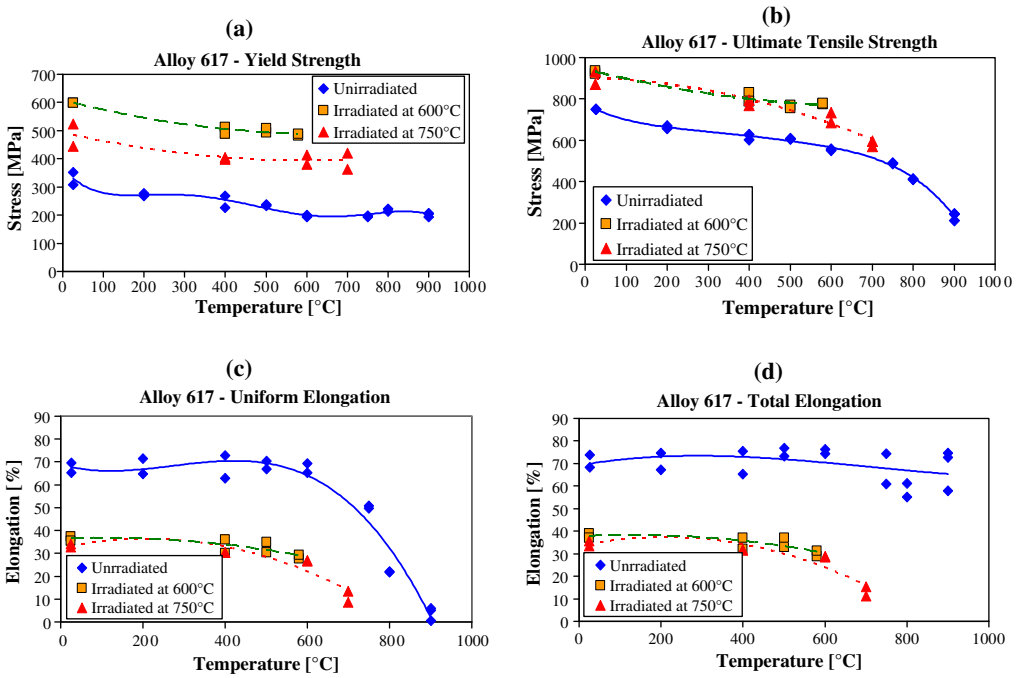

Fig. 7. Tensile test results for Alloy 617: unirradiated and after irradiation to about 1.42 dpa, (a) yield strength, (b) ultimate tensile strength, (c) uniform elongation, and (d) total elongation.

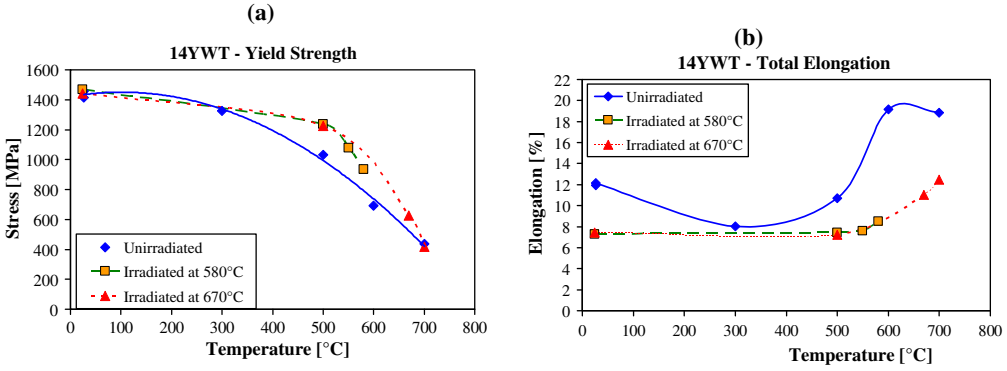

Fig. 8. Tensile test results for NFA 14YWT: unirradiated and after irradiation to about 1.25 dpa, (a) yield strength, and (b) total elongation.

For the annealed 9Cr–1MoV (Fig. 10), the irradiation-induced hardening is quite small, as expected, with hardening of about 50 MPa at both irradiation temperatures. The uniform elongation was reduced somewhat for tests up to about 600 °C, followed by a reduction to about 1% at 650 °C. For the total elongation, no changes occurred from room temperature to about 500 °C, but significant reductions occurred for tests from 550 to 650 °C. In that temperature range, the total elongation of the unirradiated material approximately doubled from that at 500 °C and lower, so the resulting irradiation effect, even at this low dose, was to eliminate the significant thermally-induced increase in elongation at the higher temperatures.

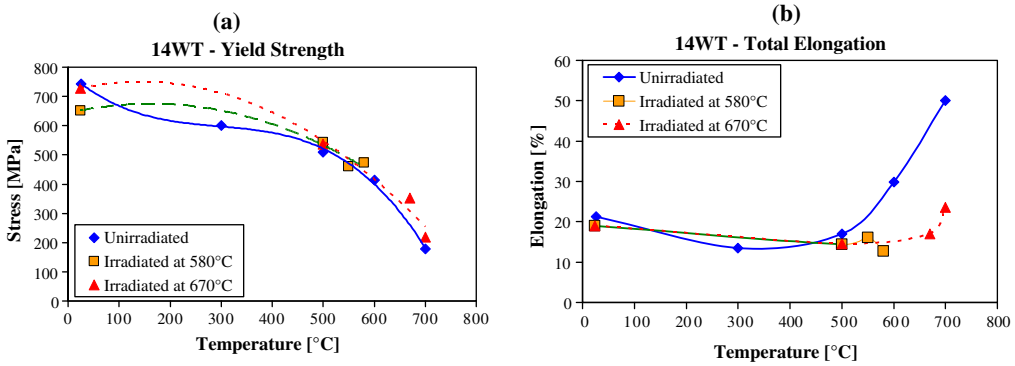

Fig. 9. Tensile test results for 14WT: unirradiated and after irradiation to about 1.25 dpa, (a) yield stress, and (b) total elongation.

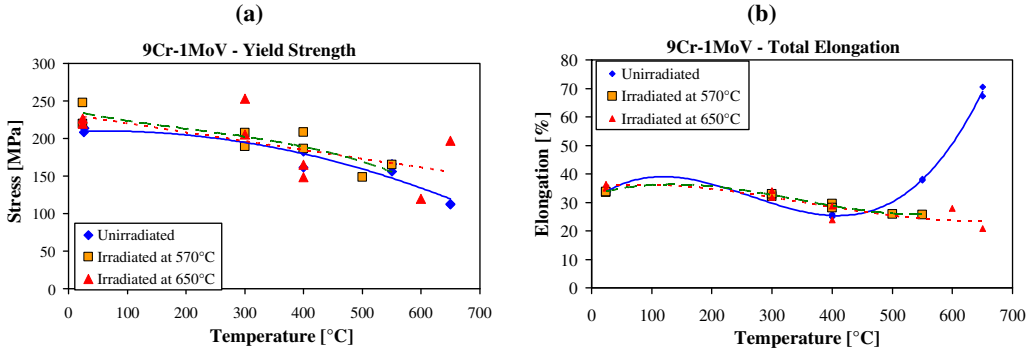

Fig. 10. Tensile test results for 9Cr–1MoV (annealed): unirradiated and after irradiation to about 1.28 dpa, (a) yield stress, and (b) total elongation.

5. Conclusions

This paper provides a summary of the results of high temperature scoping irradiations of selected Generation IV structural metallic materials. Small flat (SS-3) tensile specimens were irradiated to 1.2–1.6 dpa at 570–660 °C in rabbit capsules in the HFIR. These scoping experiments show:

1. Alloy 800H hardening resulting from the 580 °C irradiation was significant, with increases in yield and ultimate strengths on the order of 50–100%. The 660 °C irradiation produced a small amount of hardening, but with extremely low tensile elongations when tested at 700 °C. Grain boundary engineered 800H exhibited much greater hardening at 580 °C and yet retained high ductility.
2. The Alloy 617 also exhibited significant increases in yield and ultimate strength but, unlike Alloy 800H, exhibited at least 10% tensile elongation at 700 °C.
3. For the NFA 14WT and 14YWT materials, the results indicate only slight irradiation-induced hardening at this relatively low exposure, but significant decreases in tensile ductility, especially total elongation. Total elongation remained above 7% at all test temperatures to 700 °C.
4. Annealed 9Cr–1MoV shows only small amounts of irradiation-induced hardening at these doses.

Acknowledgements

The authors are grateful to Joel McDuffee and Bob Sitterson for rabbit capsule design and fabrication, Janie Myers and Eric Manneschmidt for testing assistance, Don Erdman for modification of the tensile testing software, Pat Bishop and the 3025E operators for operations in the hot cells, and Renetta Godfrey for preparation of the manuscript. Special thanks are extended to Dr Jian Gan of Idaho National Laboratory for providing the Alloy 800H.

This work was sponsored by the US Department of Energy, Office of Nuclear Energy Science and Technology under contract DE-AC05-00OR22725 with Oak Ridge National Laboratory, managed by UT-Battelle, LLC.

References

[1] Randy K. Nanstad, David A. McClintock, David T. Hoelzer, in: Proceedings of ICAPP 2007, Paper 7571, Nice, France, May 13–18, 2007.
[2] Roger E. Stoller, Louis K. Mansur, Modeling and Microstructural Analysis: Needs and Requirements for Generation IV Fission Reactors, Oak Ridge National Laboratory Report ORNL/TM-2003/242, Oak Ridge, Tennessee, May 28, 2004.
[3] J. Buongiorno et al., Supercritical Water Reactor (SCWR) Survey of Materials Experience and R&D Needs to Assess Viability, Idaho National Engineering Laboratory Report INEEL/EXT-03-00693 (Rev. 1), Idaho Falls, Idaho, September 2003.
[4] G.O. Hayner et al., Next Generation Nuclear Plant Materials Selection and Qualification Program Plan, Idaho National Engineering Laboratory Report INEEL/EXT-03-001128 (Rev. 0), Idaho Falls, Idaho, November 7, 2003.
[5] W.R. Corwin et al., The Gas Fast Reactor (GFR) Survey of Materials Experience and R&D Needs to Assess Viability, Oak Ridge National Laboratory Report ORNL/TM-2004/99, Oak Ridge, Tennessee, April 30, 2004.
[6] L.K. Mansur et al., J. Nucl. Mater. 329–333 (2004) 166.
[7] Louis K. Mansur, Randy K. Nanstad, Arthur F. Rowcliffe, Ronald L. Klueh, Survey of Metallic Materials for Irradiated Service in Generation IV Reactor Internals and Pressure Vessels, Oak Ridge National Laboratory Report, ORNL/TM-2005/519, Oak Ridge, Tennessee, submitted for publication.
[8] Randy K. Nanstad, Louis K. Mansur, Arthur Rowcliffe, Oak Ridge National Laboratory Letter Report, Plan for Qualification of Materials for Radiation Service: Generation IV Reactor Materials Program, Unpublished Report, Oak Ridge, Tennessee, August 31, 2004.
[9] A.F. Rowcliffe, Louis K. Mansur, D.T. Hoelzer, R.K. Nanstad, J. Nucl. Mater., these Proceedings.
[10] David A. McClintock, M.A. Sokolov, D.T. Hoelzer, R.K. Nanstad, J. Nucl. Mater., these Proceedings.
[11] L. Tan, K. Sridharan, T.R. Allen, R.K. Nanstad, D.A. McClintock, J. Nucl. Mater. 374 (2008) 270.
[12] D.T. Hoelzer, M.A. Sokolov, J. Bentley, M.K. Miller, R.E. Stoller, in: Effect of Particle Dispersions on Tensile Properties of Oxide Dispersion Strengthened

(ODS) and Nanostructured (NS) Ferritic Alloys, Presentation at Mat. Res. Soc. Symp., San Francisco, CA, 2005.
[13] D.T. Hoelzer, J. Bentley, M.A. Sokolov, M.K. Miller, G.R. Odette, M.J. Alinger, J. Nucl. Mater. 367–370 (2007) 166.
[14] M.K. Miller, D.T. Hoelzer, E.A. Kenik, K.F. Russell, Intermetallics 13 (2005) 387.
[15] Lance L. Snead, A. Marie Williams, A.L. Qualls, Revisiting the use of SiC as a post irradiation temperature monitor, in: M.L. Grossbeck (Ed.), Effects of Radiation on Materials, ASTM STP 1447, ASTM International, West Conshohocken, PA, 2003, p. 623.